# Spatiotemporal Analysis of Nonaffine Displacements in Disordered Solids Sheared Across the Yielding Point

NIKOLAI V. PRIEZJEV

The time evolution and spatial correlations of nonaffine displacements in deformed amorphous solids are investigated using molecular dynamics simulations. The three-dimensional model glass is represented *via* the binary mixture, which is slowly annealed well below the glass transition temperature and then sheared at a constant strain rate. It is shown that with increasing strain, the typical size of clusters of atoms with large nonaffine displacements increases, and these clusters remain spatially homogeneously distributed, until the yielding point when mobile atoms become localized within a system-spanning shear band. Furthermore, the yielding transition is associated with an abrupt change in the spatial correlation of nonaffine displacements, which varies from exponential to power-law decay. We also find that the height of the first peak in the pair correlation function of small atoms exhibits a distinct increase at the yielding strain. These results are discussed in relation to the yielding transition in amorphous materials under cyclic loading.

https://doi.org/10.1007/s11661-020-05774-5


## I. INTRODUCTION

THE atomic level understanding of the structure–property relationship of amorphous materials is important for numerous structural and biomedical applications.[1–3] By now it is well established that an elementary plastic event in disordered solids involves a collective rearrangement of a small group of neighboring particles, or the so-called shear transformation.[4,5] It was recently argued that mechanical yield in amorphous solids is a first-order phase transition from a limited set to a vast number of atomic configurations.[6] In the past, the yielding transition and the strain localization during startup deformation at a constant rate were repeatedly observed in atomistic simulation studies.[7–13] In particular, it was found that at the critical strain, the disordered systems exhibit a power-law distribution of mobile regions, which belongs to the universality class of directed percolation.[11] Remarkably, the percolation of clusters of nonaffine deformation at the yielding transition were directly observed in experiments on strained colloidal glasses.[14] More recently, molecular dynamics simulations of metallic glasses showed the exponential correlation of nonaffine displacements with a decay length that was related to the size of shear transformation zones in the elastic regime of deformation.[13] Although the yielding phenomenon in deformed disordered systems is ubiquitous, the complete picture, including the exact form of spatial correlation of nonaffine displacements and the failure mechanism, remains not fully understood.

In recent years, molecular dynamics simulations were widely used to examine structural relaxation and mechanical properties of amorphous solids subjected to time periodic deformation.[15–32] Most notably, it was found that in the athermal quasistatic limit, following a number of subyield cycles, the disordered systems reach the so-called limit cycle, a dynamic steady state of reversible particle dynamics, and, in addition, the size of clusters of particles undergoing cooperative rearrangements becomes comparable with the system size at the critical strain amplitude.[18] During periodic deformation at a finite temperature, the majority of particles undergo reversible nonaffine displacements with amplitudes that approximately follow a power-law distribution.[19,21] Interestingly, some particles were found to escape their cages temporarily while still undergoing periodic nonaffine displacements during several cycles at strain amplitudes below the critical value.[19] At sufficiently large strain amplitudes, the yielding transition occurs after a number of transient cycles for both slowly and rapidly annealed glasses, and the transition is associated with the formation of a shear band across the system and the appearance of a finite hysteresis loop.[23,26] Despite extensive studies, however, the

NIKOLAI V. PRIEZJEV is with the Department of Mechanical and Materials Engineering, Wright State University, Dayton, OH 45435. Contact e-mail: nikolai.priezjev@wright.edu
Manuscript submitted October 29, 2019.
Article published online April 28, 2020

precise determination of the critical strain amplitude and its dependence on the processing history and loading conditions remains a challenging problem.

In this paper, the microscopic analysis of particle displacements in a model glass deformed at constant strain rate is performed using molecular dynamics simulations. The binary glass is first slowly cooled well below the glass transition temperature and then strained above the yielding point. It will be shown that the stress overshoot occurs at the value of shear strain greater than the critical strain amplitude for the yielding transition during oscillatory deformation at the same density and temperature. During shear startup, atoms with large nonaffine displacements form clusters that are homogeneously distributed in space, until they suddenly become localized at the yielding strain. Moreover, the yielding transition is signaled by a distinct change in the shape of the probability distribution of the nonaffine measure, spatial correlations of nonaffinity, and the peak height of the pair correlation function.

The rest of the paper is structured as follows. The details of molecular dynamics simulations are given in the next section. The spatial and temporal analysis of nonaffine displacements, the stress response, and the pair correlation function are presented in Section III. The results are summarized in the last section.

## II. MOLECULAR DYNAMICS SIMULATIONS

The molecular dynamics simulations are performed on a well-studied system of two types of atoms (80:20) that have strongly non-additive interaction, which prevents crystallization upon cooling.[33] The binary mixture model was first introduced and extensively studied by Kob and Andersen (KA) about 20 years ago.[33] The interaction parameters of the KA mixture are similar to the parametrization used by Weber and Stillinger to study the amorphous metal-metalloid alloy $Ni_{80}P_{20}$.[34] In the KA model, the interaction between atoms of types $\alpha$, $\beta = A, B$ is specified *via* the Lennard–Jones (LJ) potential, as follows:

$$V_{\alpha\beta}(r) = 4\,\varepsilon_{\alpha\beta}\left[\left(\frac{\sigma_{\alpha\beta}}{r}\right)^{12} - \left(\frac{\sigma_{\alpha\beta}}{r}\right)^{6}\right], \qquad [1]$$

where the parameters are set to $\varepsilon_{AA} = 1.0$, $\varepsilon_{AB} = 1.5\ \varepsilon_{BB} = 0.5$, $\sigma_{AA} = 1.0$, $\sigma_{AB} = 0.8$, $\sigma_{BB} = 0.88$, and $m_A = m_B$.[33] The LJ potential is truncated at the cutoff radius $r_{c,\alpha\beta} = 2.5\,\sigma_{\alpha\beta}$ to alleviate the computational efforts. In what follows, the simulation results are reported in the reduced LJ units of length, mass, energy, and time: $\sigma = \sigma_{AA}$, $m = m_A$, $\varepsilon = \varepsilon_{AA}$, and $\tau = \sigma\sqrt{m/\varepsilon}$, respectively. The equations of motion for each atom were integrated using the velocity-Verlet algorithm with the time step $\triangle t_{MD} = 0.005\,\tau$.[35,36]

We next describe the equilibration procedure and the shear strain deformation protocol. All simulations were carried out at constant volume with the corresponding density $\rho = \rho_A + \rho_B = 1.2\,\sigma^{-3}$. The system size is $L = 36.84\,\sigma$ and the total number of atoms is 60 000. The binary mixture was first equilibrated in the liquid state at the temperature $T_{LJ} = 1.0\,\varepsilon/k_B$, where $k_B$ denotes the Boltzmann constant. The temperature was regulated *via* the Nosé-Hoover thermostat,[35,36] and the periodic boundary conditions were applied along all three spatial dimensions. The computer glass transition temperature of the KA model at $\rho = 1.2\,\sigma^{-3}$ is $T_c = 0.435\,\varepsilon/k_B$.[33] Following the equilibration at $T_{LJ} = 1.0\,\varepsilon/k_B$, the system was cooled down to $T_{LJ} = 0.01\,\varepsilon/k_B$ with the computationally slow rate of $10^{-5}\varepsilon/k_B\tau$ at constant volume. The independent glass samples were prepared by generating 100 different atomic configurations at the temperature $T_{LJ} = 1.0\,\varepsilon/k_B$, which were linearly cooled with the rate $10^{-5}\varepsilon/k_B\tau$ to the low temperature $T_{LJ} = 0.01\,\varepsilon/k_B$. Once at $T_{LJ} = 0.01\,\varepsilon/k_B$, the glass was strained along the $xz$ plane with the constant shear rate $10^{-5}\,\tau^{-1}$ up to $\gamma_{xz} = 0.20$, using the Lees–Edwards boundary conditions.[36] During strain deformation, the potential energy, stress components, and atomic configurations were periodically saved for further analysis.

## III. RESULTS

It is well realized by now that the mechanical response of disordered solids under applied strain involves a series of rapid rearrangements of clusters of particles that in turn induce long-range deformation fields.[1] In general, the atomic level description of such processes is complicated due to the spatial overlap of the deformation fields and a wide distribution of the local yield stresses. More recently, this problem was addressed by constructing elastoplastic models where a disordered system is represented *via* a collection of interacting blocks with certain elastic properties and a distribution of yield thresholds.[1] In the present study, we revisit the problem of startup deformation of amorphous materials using molecular dynamics simulations and report our observations in terms of nonaffine displacements of atoms in the vicinity of the yielding transition.

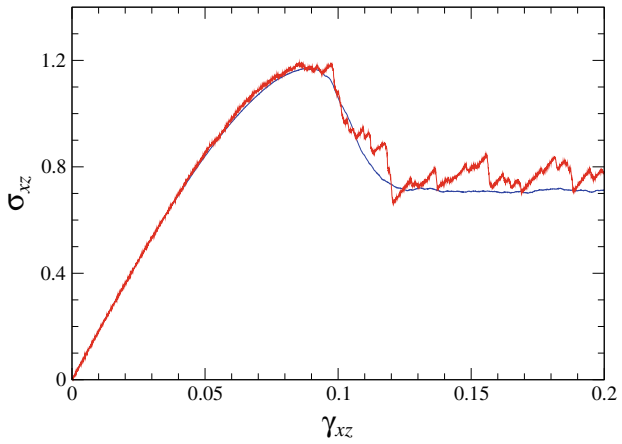


Fig. 1—(Color online) The shear stress $\sigma_{xz}$ (in units of $\varepsilon\sigma^{-3}$) as a function of strain up to $\gamma_{xz} = 0.20$. The data are taken in one sample (the red curve) and averaged over 100 samples (the blue curve). The shear rate is $\dot{\gamma}_{xz} = 10^{-5}\,\tau^{-1}$ and temperature is $T_{LJ} = 0.01\,\varepsilon/k_B$.

The dependence of shear stress as a function of strain is presented in Figure 1 for the deformed glass with the constant strain rate of $10^{-5}\,\tau^{-1}$. The data are collected either in one sample (the red curve) or averaged over 100 independent samples (the blue curve). As is evident, the stress-strain curve for one sample is punctuated by a series of abrupt stress drops that are characteristic of sudden rearrangements of clusters of atoms. In both cases, the stress response exhibits a linear regime of deformation at small strain and a pronounced yielding peak at about $\gamma_{xz} \approx 0.09$, followed by a nearly constant stress level at higher strain. The appearance of the stress overshoot is the signature of a relatively slow cooling from the liquid state and/or an extended annealing period below the glass transition temperature, when the glass is settled in a sufficiently deep energy well. This behavior was repeatedly observed in the previous MD simulations.[7,11,12,22]

It should be commented that the value $\gamma_{xz} \approx 0.09$ is larger than the critical strain amplitude for yielding during oscillatory shear deformation of the KA binary glass at the same density and temperature.[23] It was previous shown that the critical strain amplitude of the KA mixture is in the range $0.07 < \gamma_0 < 0.08$ at the density $\rho = 1.2\,\sigma^{-3}$ in athermal quasistatic (the limiting case of $T_{\mathrm{LJ}} = 0$ and $\dot{\gamma}_{xz} = 0$) simulations.[16,22] Moreover, it was demonstrated that the yielding transition occurs after about 20 shear cycles at the strain amplitude $\gamma_0 = 0.08$, when $\rho = 1.2\,\sigma^{-3}$ and $T_{\mathrm{LJ}} = 0.01\,\varepsilon/k_{\mathrm{B}}$ for glasses prepared with the slow cooling rate $10^{-5}\varepsilon/k_{\mathrm{B}}\tau$.[23] The periodic loading resulted in a gradual increase of the potential energy due to accumulation of irreversible rearrangements, followed by the formation of the shear band during three consecutive shear cycles.[23] For reference, the oscillation period in the previous study on the KA glass was set to $5000\,\tau$, and, therefore, the shear rate at zero strain was equal to $10^{-4}\,\tau^{-1}$.[23] More recently, simulations of the poorly-annealed binary mixture at higher temperature $T_{\mathrm{LJ}} = 0.1\,\varepsilon/k_{\mathrm{B}}$ and $\rho = 1.2\,\sigma^{-3}$ have shown that the yielding transition occurs after about 150 shear cycles at lower strain amplitude $\gamma_0 = 0.06$.[26] Overall, these results confirm that the critical strain amplitude is reduced upon increasing temperature.[15,22,23,26]

Figure 2 shows the shear modulus and yielding peak as a function of the potential energy at zero strain for 100 independent samples. Here, the values of the potential energy are reported for the samples cooled with the rate $10^{-5}\varepsilon/k_{\mathrm{B}}\tau$ to the temperature $T_{\mathrm{LJ}} = 0.01\,\varepsilon/k_{\mathrm{B}}$ at $\rho = 1.2\,\sigma^{-3}$. The variation of the data is related to different energy minima in the potential energy landscape probed by the annealing of independent samples. In turn, the shear modulus was computed from the linear slope of the stress-strain curves at $\gamma_{xz} \leqslant 0.01$, whereas the height of the yielding peak was evaluated by averaging the local maximum of the shear stress for each sample. The averaged values of the shear modulus and the stress overshoot are $G = 18.3 \pm 0.2\,\varepsilon\sigma^{-3}$ and $\sigma_Y = 1.19 \pm 0.02\,\varepsilon\sigma^{-3}$, respectively. The data are somewhat scattered but the trend can be clearly identified *via* the negative slopes of the red lines that represent the best linear fit to the data points. In other words, samples annealed to lower energy states tend to have larger values of $G$ and $\sigma_Y$.

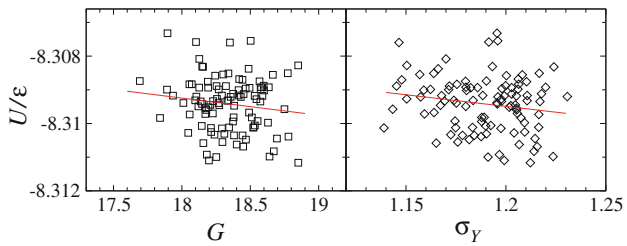


Fig. 2—(Color online) The shear modulus $G$ (in units of $\varepsilon\sigma^{-3}$, left panel) and the yielding peak $\sigma_Y$ (in units of $\varepsilon\sigma^{-3}$, right panel) *vs* the potential energy at zero strain for 100 independent samples. The red lines are the best fit to the data.

The microscopic details of the deformation process in disordered solids can be unveiled *via* the analysis of the so-called nonaffine displacements of atoms. Unlike crystalline materials, where the displacement of individual atoms can be defined with respect to the periodic lattice, the description of atomic rearrangements in amorphous materials is based on the relative displacements of atoms with respect to their neighbors. More specifically, the nonaffine displacement of an atom $i$ is defined *via* the matrix $\mathbf{J}_i$, which transforms the neighboring atoms during the time interval $\Delta t$ and, at the same time, minimizes the quantity:

$$D^2(t,\Delta t) = \frac{1}{N_i}\sum_{j=1}^{N_i}\Big\{\mathbf{r}_j(t+\Delta t) - \mathbf{r}_i(t+\Delta t) - \mathbf{J}_i\big[\mathbf{r}_j(t) - \mathbf{r}_i(t)\big]\Big\}^2, \qquad [2]$$

where the summation is performed over atoms within the distance of $1.5\,\sigma$ from the position of the $i$-th atom at $\mathbf{r}_i(t)$. This quantity was first used by Falk and Langer to unambiguously identify the local shear transformations in deformed disordered solids.[37] Since then, the spatiotemporal analysis of nonaffine displacements was extensively applied to investigate the structural relaxation in amorphous solids strained with a constant rate[13,38–41] and periodically deformed.[19,21,23,25–27,32,42,43] In general, it was found that subyield cyclic deformation leads to the appearance of finite clusters of atoms with large nonaffine displacements, and the size of these clusters is reduced with increasing cycle number, when the system gradually approaches a certain potential energy level.[25–27] On the other hand, at sufficiently large strain amplitude, the yielding transition occurs *via* the formation of a shear band, typically after a number of transient cycles.[22,23,26]

The representative snapshots of the strained glass are displayed in Figure 3 for the values of shear strain $\gamma_{xz} = 0.05$, 0.10, 0.15, and 0.20. In each case, the nonaffine measure, given by Eq. [2], was computed with respect to the atomic configuration at zero strain. Note that, the snapshots in Figure 3 are taken for the same sample as the stress–strain curve (the red curve) shown in Figure 1. It can be clearly seen from Figure 3 that shear deformation is initially nearly homogeneous, and then it

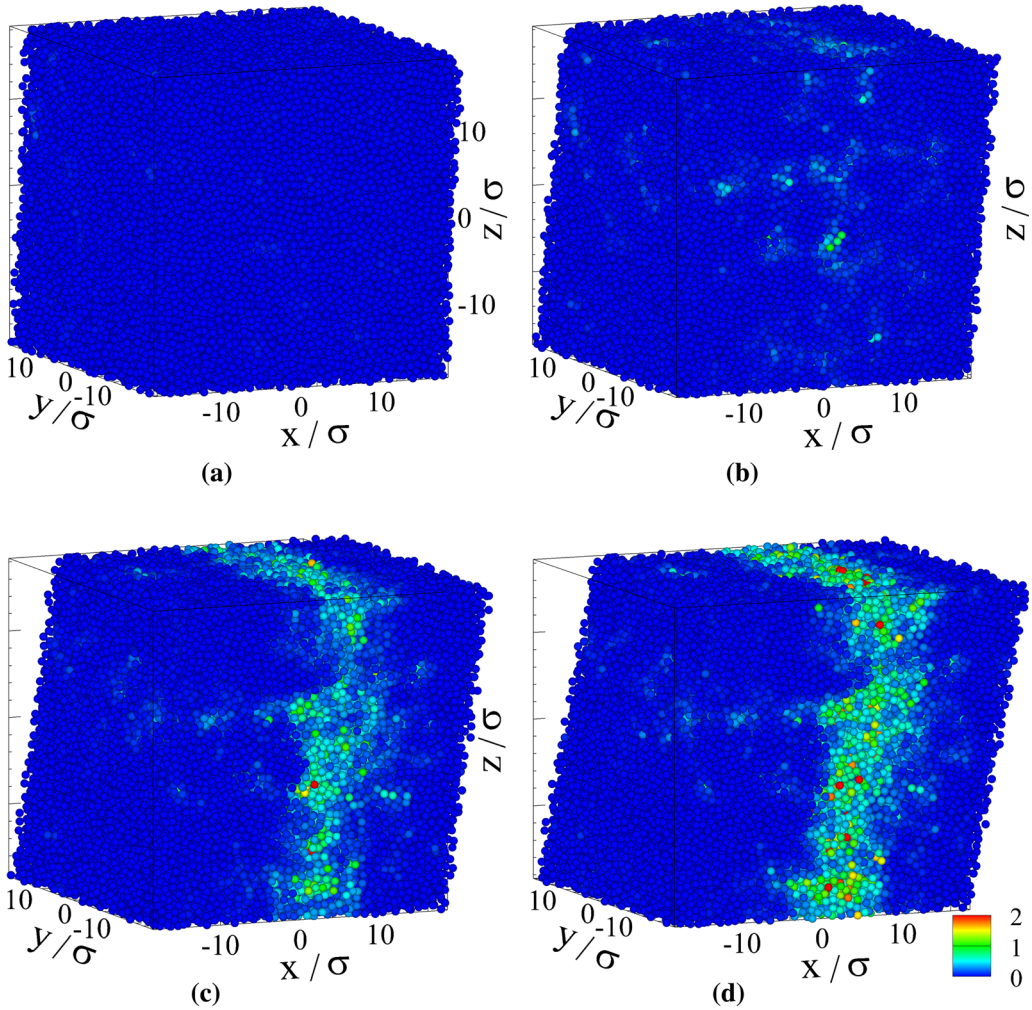


Fig. 3—(Color online) The sequence of snapshots of the binary glass strained along the $xz$ plane with the rate $10^{-5}\,\tau^{-1}$. The shear strain is (*a*) 0.05, (*b*) 0.10, (*c*) 0.15, and (*d*) 0.20. The color denotes $D^2$ with respect to $\gamma_{xz} = 0$, as indicated in the legend. Atoms are not shown to scale.

proceeds *via* the formation of the shear band across the system with the width of several atomic diameters. The unusual orientation of the shear band in this particular sample is allowed due to the periodic boundary conditions.

A more detailed analysis of spatial configurations of atoms with large nonaffine displacements near the yielding point is shown in Figure 4 for strains $\gamma_{xz} =$ 0.05, 0.06, 0.07, and 0.08 and in Figure 5 for $\gamma_{xz} = 0.09$, 0.10, 0.11, and 0.12. In Figures 4 and 5, only the positions of atoms with $D^2(0, \Delta t) > 0.04\,\sigma^2$ are displayed for clarity. The threshold value for the nonaffine measure was chosen to be slightly larger than the typical cage size $r_c \approx 0.1\,\sigma$. It can be observed that finite clusters of mobile atoms are already formed at relatively small values of strain, *i.e.*, $\gamma_{xz} \leqslant 0.07$, see Figures 4(a) through (c). Furthermore, at the higher strain $\gamma_{xz} = 0.08$, the clusters of atoms form a larger network, which is nearly homogeneously distributed in the sample, see Figure 4(d). Upon increasing strain, the shear band forms along the plane at $x \approx 5\,\sigma$ when $\gamma_{xz} = 0.09$, as shown in Figure 5(a). As evident in Figure 5, the shear band becomes fully developed at higher strain $\gamma_{xz} \geqslant 0.10$.

The quantitative analysis of the spatial and temporal evolution of nonaffine displacements involves a sequence of spatially averaged profiles of $D^2(x)$ within narrow bins of thickness $\Delta x = \sigma$. The results are presented in Figure 6 for the values of shear strain $\gamma_{xz} \leqslant$ 0.10. It can be clearly seen that the average level of $D^2(x)$ becomes higher when $\gamma_{xz}$ increases, until $\gamma_{xz} =$ 0.09 when a pronounced peak is developed reflecting the formation of the shear band. In principle, one can assume that the location of a shear band can be predicted from the spatial patterns of large nonaffine displacements at shear strains smaller than the yielding point. The results in Figure 6 show, however, that generally this is not the case. For example, the profile at $\gamma_{xz} = 0.08$ (denoted by the dashed curve in Figure 6) contains two local maxima at $x \approx -10\,\sigma$ and $x \approx 8\,\sigma$. Despite that the former maximum is slightly higher at $\gamma_{xz} = 0.08$, the shear band is formed at the location of the latter maximum when $\gamma_{xz} = 0.09$, see Figure 6. Altogether, these results indicate that the yielding

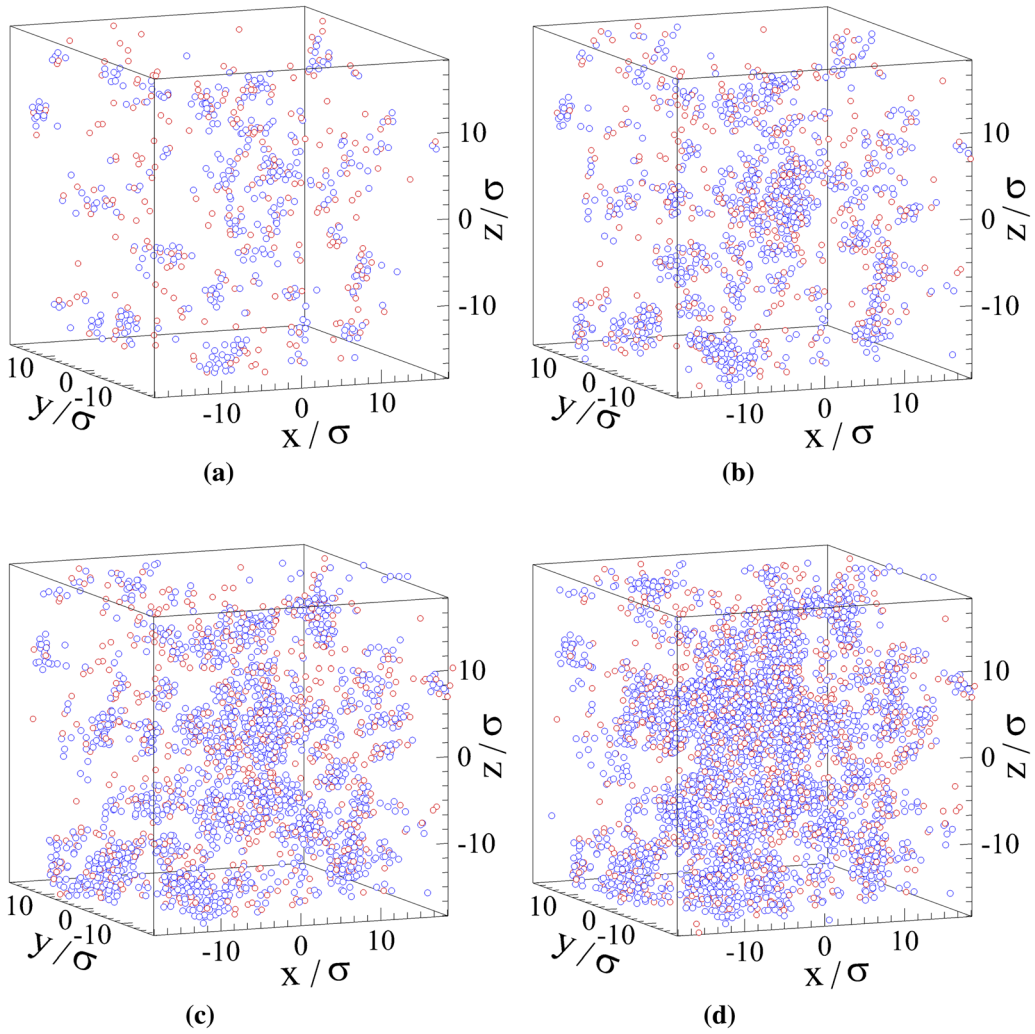


Fig. 4—(Color online) The spatial configurations of atoms $A$ (blue spheres) and $B$ (red spheres) with the nonaffine measure: (*a*) $D^2(0, 5 \times 10^3\tau) > 0.04\,\sigma^2$, (*b*) $D^2(0, 6 \times 10^3\tau) > 0.04\,\sigma^2$, (*c*) $D^2(0, 7 \times 10^3\tau) > 0.04\,\sigma^2$, and (*d*) $D^2(0, 8 \times 10^3\tau) > 0.04\,\sigma^2$. The shear strain is (a) 0.05, (b) 0.06, (c) 0.07, and (d) 0.08. The glass is strained along the $xz$ plane with the rate $10^{-5}\,\tau^{-1}$.

transition is associated with an abrupt change from a nearly homogeneous distribution of clusters of atoms with large nonaffine displacements to a localization within a narrow region. Note that qualitatively similar conclusions were obtained for both well and poorly annealed glasses subjected to oscillatory shear deformation.[23,26]

The normalized probability distribution function (PDF) of the quantity $D^2$ is presented in Figure 7 for the values of the shear strain in the range $0.01 \leqslant \gamma_{xz} \leqslant 0.10$. As in the previous analysis, the nonaffine displacements for each sample were computed with respect to atomic positions at zero strain. It can be noticed that even at small strain $\gamma_{xz} = 0.01$, some atoms undergo large nonaffine displacements, $D^2 \approx 0.1\,\sigma^2$, and thus leave their cages. As expected, the distribution function becomes wider with increasing shear strain. The relative increase in width becomes larger at $\gamma_{xz} = 0.10$, which is consistent with an abrupt increase in the peak height reported in Figure 6 at $\gamma_{xz} = 0.10$.

The spatial correlations of nonaffine displacements in a sheared glass can be evaluated *via* the normalized, equal-time correlation function as follows:

$$C_{D^2}(\Delta\mathbf{r}) = \frac{\langle D^2(\mathbf{r} + \Delta\mathbf{r}) D^2(\mathbf{r})\rangle - \langle D^2(\mathbf{r})\rangle^2}{\langle D^2(\mathbf{r})^2\rangle - \langle D^2(\mathbf{r})\rangle^2}, \qquad [3]$$

where the brackets indicate averaging over all pairs of atoms.[38,39] In our study, the correlation function was further averaged over 100 independent samples for each value of shear strain. The results are shown in Figure 8 for strains $\gamma_{xz} \leqslant 0.10$. It can be observed that the correlation of nonaffine displacements becomes increasingly long ranged at higher strain. The decay of the correlation function changes from exponential at $\gamma_{xz} \leqslant 0.07$ (see the same data on the log-normal scale in the inset to Figure 8) to the power-law decay with the exponent approaching $-1$ at $\gamma_{xz} = 0.10$. The tails of the power-law decay are strongly affected by the finite system size, suggesting that simulations of larger systems

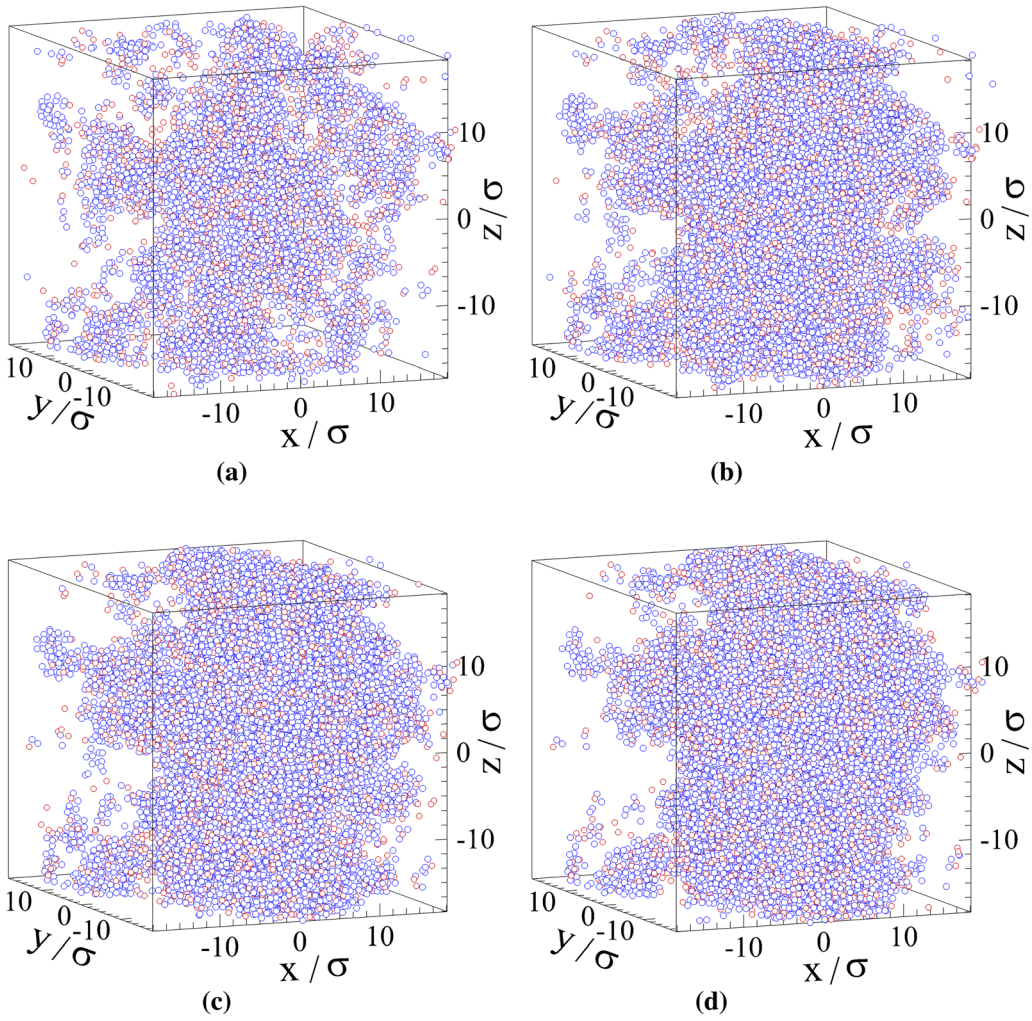


Fig. 5—(Color online) The consecutive snapshots of sheared glass at strains (*a*) 0.09, (*b*) 0.10, (*c*) 0.11, and (*d*) 0.12. The nonaffine measure: (a) $D^2(0, 9 \times 10^3\tau) > 0.04\,\sigma^2$, (b) $D^2(0, 10 \times 10^3\tau) > 0.04\,\sigma^2$, (c) $D^2(0, 11 \times 10^3\tau) > 0.04\,\sigma^2$, and (d) $D^2(0, 12 \times 10^3\tau) > 0.04\,\sigma^2$. The shear rate is $10^{-5}\,\tau^{-1}$.

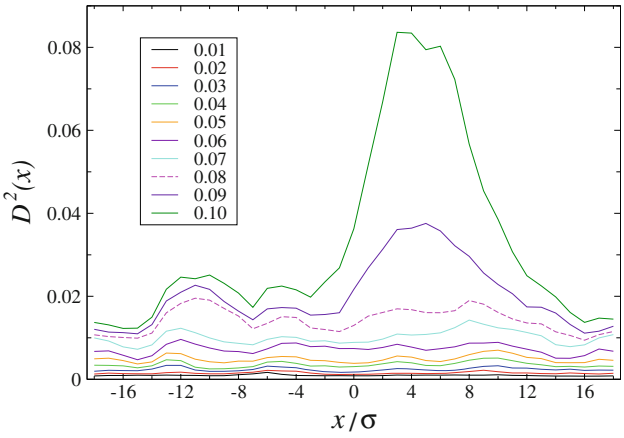


Fig. 6—(Color online) The spatial variation of the nonaffine measure $D^2(x)$ for the indicated values of the shear strain. The quantity $D^2(x)$ is computed in one sample with respect to an atomic configuration at zero strain. See text for details.

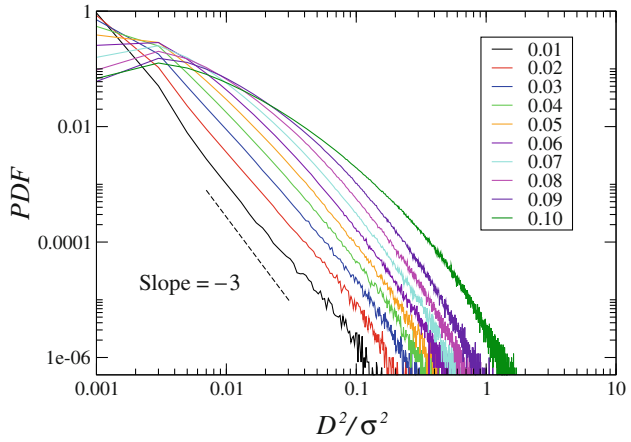


Fig. 7—(Color online) The normalized probability distribution function (PDF) of $D^2$ for the listed values of shear strain. The dashed line denotes the slope − 3. The data are averaged over 100 samples.

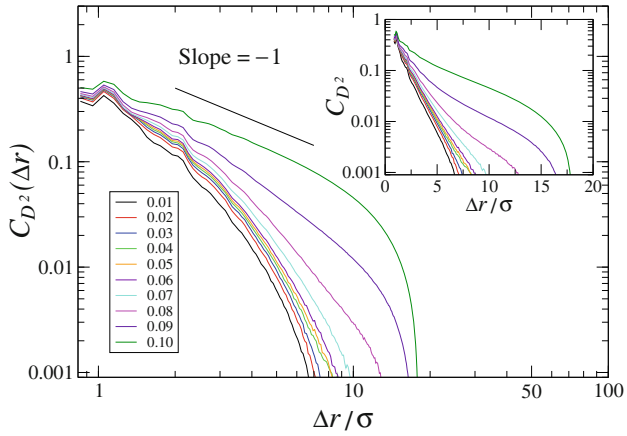


Fig. 8—(Color online) The spatial correlation function $C_{D^2}(\mathbf{\Delta r})$ defined by Eq. [3] for the indicated values of shear strain. The straight line with the slope −1 is shown for reference. Inset: The same data are replotted on the log-normal scale. The data are averaged over 100 samples.

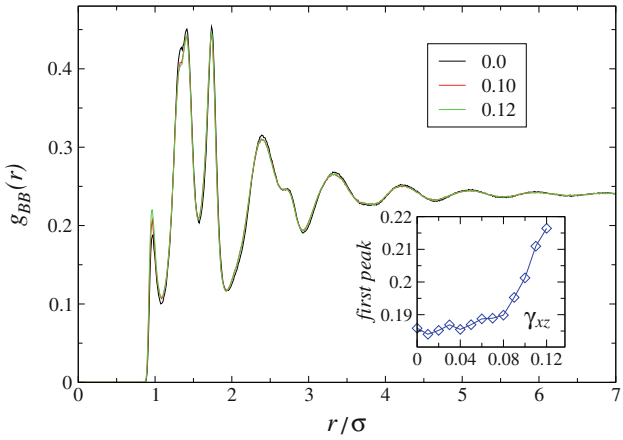


Fig. 9—(Color online) The pair correlation function, $g_{BB}(r)$, for shear strain $\gamma_{xz} = 0$, 0.10, and 0.12. The data are averaged over 100 independent samples. The inset shows the height of the first peak as a function of shear strain.

might show long range correlations more clearly. Nevertheless, it can be concluded that upon increasing strain up to $\gamma_{xz} = 0.08$, the longer correlation range is consistent with larger size of typical clusters of mobile atoms (*e.g.*, see Figure 4). Furthermore, the formation of the shear band is associated with a relatively large increase in $C_{D^2}(\mathbf{\Delta r})$ when $\gamma_{xz}$ increases from 0.08 to 0.09 (see Figure 8). We also comment that it was previously shown that thermal fluctuations in quiescent glasses lead to the exponential decay of $C_{D^2}(\mathbf{\Delta r})$, indicating that correlations of thermally-induced nonaffine rearrangements extend up to nearest-neighbor distances.[21]

We finally examine structural changes in binary glasses during startup deformation. It was previously demonstrated that in contrast to Zr-based metallic glasses, where the icosahedral short-range order is an important structural measure, the atomic structure of the KA binary glass is sensitive to the shape of the pair correlation function of smaller atoms.[41,44–46] Recall that the interaction energy $\varepsilon_{BB}$ in the LJ potential is smaller than $\varepsilon_{AA}$ and $\varepsilon_{AB}$, and, therefore, the probability of observing a neighboring pair of small atoms of type *B* is lower in well-annealed (low energy) samples. The averaged pair correlation function, $g_{BB}(r)$, is presented in Figure 9 for strains $\gamma_{xz} = 0$, 0.10, and 0.12. As is evident, the height of the first peak is the lowest in undeformed samples, and it becomes higher in strained glasses ($\gamma_{xz} = 0.10$ and 0.12) when atoms within a shear band made several cage jumps. Moreover, the dependence of the first peak height as a function of strain is reported in the inset of Figure 9. It can be seen that a distinct increase in height coincides with the formation of the shear band at $\gamma_{xz} = 0.09$. This behavior is consistent with the development of the main peak in the profile $D^2(x)$ at $\gamma_{xz} = 0.09$ shown in Figure 6 and the strain localization reported in Figure 5(a).

## IV. CONCLUSIONS

In summary, molecular dynamics simulations were carried out to study the stress response and statistical properties of nonaffine displacements during startup deformation of an amorphous solid. The binary glass was prepared by slow annealing well below the glass transition temperature at constant volume and then strained at constant deformation rate. It was shown that atoms with nonaffine displacements larger than the cage size form clusters that grow and remain homogeneously distributed in space until the yielding transition, which is associated with the formation of a localized shear band. This phenomenon is reflected in the variation of the spatial correlations of nonaffine displacements, which change from exponential to power-law decay near the yielding point. In addition, the formation of a shear band coincides with a distinct increase in the height of the first peak of the pair correlation function of small atoms. Finally, the yielding transition during startup deformation occurs at a value of shear strain greater than the critical strain amplitude of oscillatory shear deformation at the same density and temperature.

## ACKNOWLEDGMENTS

Financial support from the National Science Foundation (CNS-1531923) and the ACS Petroleum Research Fund (60092-ND9) is gratefully acknowledged. The molecular dynamics simulations were carried out using the LAMMPS code developed at Sandia National Laboratories.[35] The numerical simulations were performed at Wright State University's Computing Facility and the Ohio Supercomputer Center.

## REFERENCES


1. A. Nicolas, E.E. Ferrero, K. Martens, and J.-L. Barrat: *Rev. Mod. Phys.*, 2018, vol. 90, art. no. 045006.
2. S. Chen, J. Wang, L. Xia, and Y. Wu: *Entropy*, 2019, vol. 21, art. no. 54.
3. A. Mehjabeen, T. Song, W. Xu, H.P. Tang, and M. Qian: *Adv. Eng. Mater.*, 2018, vol. 20, art. no. 1800207.
4. F. Spaepen: *Acta Metall.*, 1977, vol. 25, pp. 407–15.
5. A.S. Argon: *Acta Metall.*, 1979, vol. 27, pp. 47–58.
6. P.K. Jaiswal, I. Procaccia, C. Rainone, and M. Singh: *Phys. Rev. Lett.*, 2016, vol. 116, art. no. 085501.
7. F. Varnik, L. Bocquet, and J.-L. Barrat: *J. Chem. Phys.*, 2004, vol. 120, pp. 788–801.
8. Y. Shi and M.L. Falk: *Phys. Rev. E*, 2006, vol. 73, art. no. 214201.
9. N.B. Bailey, J. Schiotz, and K.W. Jacobsen: *Phys. Rev. B*, 2006, vol. 73, art. no. 064108.
10. S. Ogata, F. Shimizu, J. Li, M. Wakeda, and Y. Shibutani: *Intermetallics*, 2006, vol. 14, pp. 1033–37.
11. G.P. Shrivastav, P. Chaudhuri, and J. Horbach: *Phys. Rev. E*, 2016, vol. 94, art. no. 042605.
12. G.P. Shrivastav, P. Chaudhuri, and J. Horbach: *J. Rheol.*, 2016, vol. 60, pp. 835–47.
13. R. Jana and L. Pastewka: *J. Phys. Mater.*, 2019, vol. 2, art. no. 045006.
14. A. Ghosh, Z. Budrikis, V. Chikkadi, A.L. Sellerio, S. Zapperi, and P. Schall: *Phys. Rev. Lett.*, 2017, vol. 118, art. no. 148001.
15. N.V. Priezjev: *Phys. Rev. E*, 2013, vol. 87, art. no. 052302.
16. D. Fiocco, G. Foffi, and S. Sastry: *Phys. Rev. E*, 2013, vol. 88, art. no. 020301.
17. N.V. Priezjev: *Phys. Rev. E*, 2014, vol. 89, art. no. 012601.
18. I. Regev, J. Weber, C. Reichhardt, K.A. Dahmen, and T. Lookman: *Nat. Commun.*, 2015, vol. 6, art. no. 8805.
19. N.V. Priezjev: *Phys. Rev. E*, 2016, vol. 93, art. no. 013001.
20. T. Kawasaki and L. Berthier: *Phys. Rev. E*, 2016, vol. 94, art. no. 022615.
21. N.V. Priezjev: *Phys. Rev. E*, 2016, vol. 94, art. no. 023004.
22. P. Leishangthem, A.DS. Parmar, and S. Sastry: *Nat. Commun.*, 2017, vol. 8, art. no. 14653.
23. N.V. Priezjev: *Phys. Rev. E*, 2017, vol. 95, art. no. 023002.
24. M. Fan, M. Wang, K. Zhang, Y. Liu, J. Schroers, M.D. Shattuck, and C.S. O'Hern: *Phys. Rev. E*, 2017, vol. 95, art. no. 022611.
25. N.V. Priezjev: *J. Non-Cryst. Solids*, 2018, vol. 479, pp. 42–48.
26. N.V. Priezjev: *Comput. Mater. Sci.*, 2018, vol. 150, pp. 162–68.
27. N.V. Priezjev: *Comput. Mater. Sci.*, 2018, vol. 153, pp. 235–40.
28. I. Regev, C. Reichhardt, and C.J.O. Reichhardt: *Model. Simul. Mater. Sci. Eng.*, 2019, vol. 27, art. no. 084004.
29. N.V. Priezjev and M.A. Makeev: *J. Non-Cryst. Solids*, 2019, vol. 506, pp. 14–20.
30. N.V. Priezjev and M.A. Makeev: *Model. Simul. Mater. Sci. Eng.*, 2019, vol. 27, art. no. 025004.
31. K. Nagasawa, K. Miyazaki, and T. Kawasaki: *Soft Matter*, 2019, vol. 15, pp. 7557–66.
32. N.V. Priezjev: *J. Non-Cryst. Solids*, 2019, vol. 525, art. no. 119683.
33. W. Kob and H.C. Andersen: *Phys. Rev. E*, 1995, vol. 51, pp. 4626–41.
34. T.A. Weber and F.H. Stillinger: *Phys. Rev. B*, 1985, vol. 31, pp. 1954–63.
35. S.J. Plimpton: *J. Comput. Phys.*, 1995, vol. 117, pp. 1–19.
36. M.P. Allen and D.J. Tildesley: *Computer Simulation of Liquids*, Clarendon, Oxford, 1987.
37. M.L. Falk and J.S. Langer: *Phys. Rev. E*, 1998, vol. 57, pp. 7192–7205.
38. V. Chikkadi and P. Schall: *Phys. Rev. E*, 2012, vol. 85, art. no. 031402.
39. F. Varnik, S. Mandal, V. Chikkadi, D. Denisov, P. Olsson, D. Vagberg, D. Raabe, and P. Schall: *Phys. Rev. E*, 2014, vol. 89, art. no. 040301.
40. J. Ding, Y.Q. Cheng, and E. Ma: *Appl. Phys. Lett.*, 2012, vol. 101, art. no. 121917.
41. N.V. Priezjev: *Comput. Mater. Sci.*, 2020, vol. 174, art. no. 109477.
42. N.V. Priezjev: *J. Non-Cryst. Solids*, 2019, vol. 503, pp. 131–38.
43. N.V. Priezjev: *Comput. Mater. Sci.*, 2019, vol. 168, pp. 125–30.
44. M. Utz, P.G. Debenedetti, and F.H. Stillinger: *Phys. Rev. Lett.*, 2000, vol. 84, pp. 1471–74.
45. K. Vollmayr, W. Kob, and K. Binder: *J. Chem. Phys.*, 1996, vol. 105, pp. 4714–28.
46. N.V. Priezjev: *J. Non-Cryst. Solids*, 2019, vol. 518, pp. 128–33.